USGS
science for a changing world

Prepared in cooperation with Northern Arizona University and Marda Science LLC

Channel Mapping of the Colorado River from Glen Canyon Dam to Lees Ferry in Glen Canyon National Recreation Area, Arizona

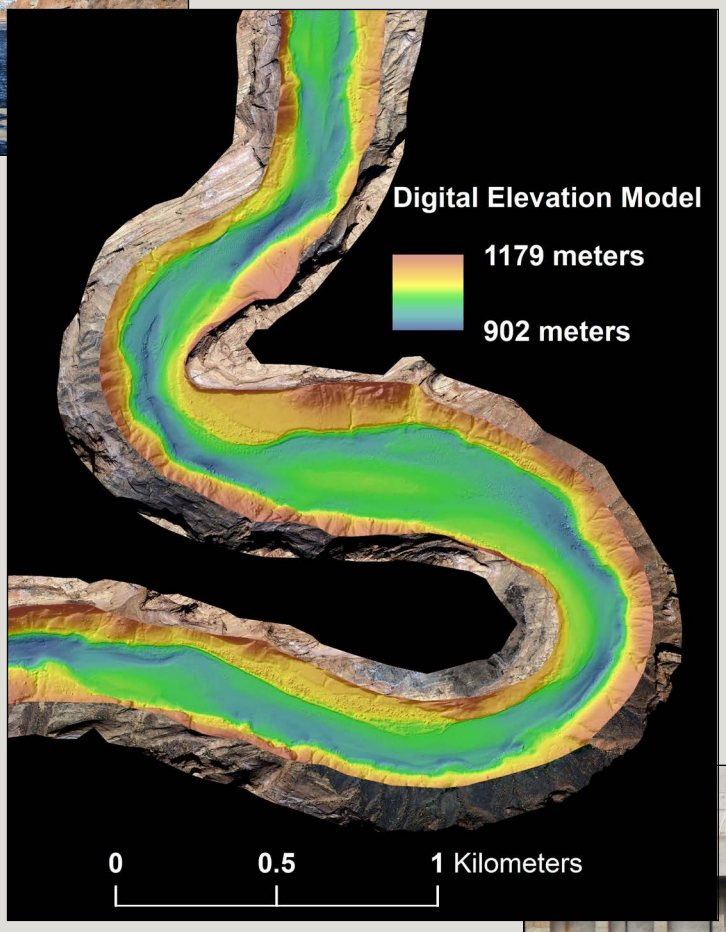

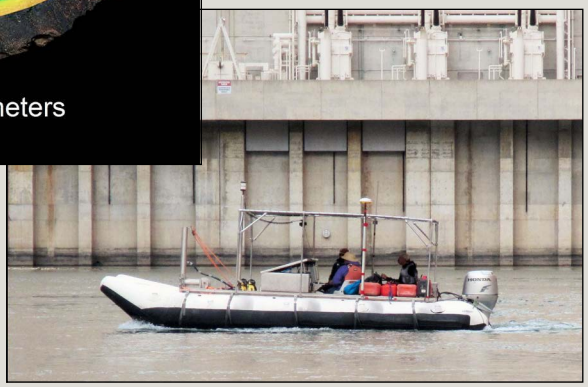

Open-File Report 2022–1057

U.S. Department of the Interior
U.S. Geological Survey

Cover. (top left) Photograph of Ryan Seumptewa conducting total station topographic survey in a shallow area near Glen Canyon Dam (photograph by Matt Kaplinski, Northern Arizona University); (middle) digital elevation model of the "Big Bend" area of Glen Canyon (Kaplinski and others, 2022; https://doi.org/10.5066/P98GFP93), overlain on orthophotograph collected in 2013; (bottom right) photograph of research vessel RV *Greg Sponenbergh* conducting multibeam sonar survey near Glen Canyon Dam (photograph by Keith Kohl, U.S. Geological Survey).

Channel Mapping of the Colorado River from Glen Canyon Dam to Lees Ferry in Glen Canyon National Recreation Area, Arizona

By Matt Kaplinski, Joseph E. Hazel, Jr., Paul E. Grams, Tom Gushue, Daniel D. Buscombe, and Keith Kohl

Prepared in cooperation with Northern Arizona University and Marda Science LLC

Open-File Report 2022–1057

U.S. Department of the Interior
U.S. Geological Survey

U.S. Geological Survey, Reston, Virginia: 2022

For more information on the USGS—the Federal source for science about the Earth, its natural and living resources, natural hazards, and the environment—visit https://www.usgs.gov or call 1–888–ASK–USGS.

For an overview of USGS information products, including maps, imagery, and publications, visit https://store.usgs.gov.

Suggested citation:
Kaplinski, M., Hazel, J.E., Jr., Grams, P.E., Gushue, T., Buscombe, D.D., and Kohl, K., 2022, Channel mapping of the Colorado River from Glen Canyon Dam to Lees Ferry in Glen Canyon National Recreation Area, Arizona: U.S. Geological Survey Open-File Report 2022–1057, 20 p., https://doi.org/10.3133/ofr20221057.

Associated data for this publication:
Kaplinski, M., Hazel, J.E., Jr., Grams, P.E., Gushue, T., Buscombe, D.D., and Kohl, K., 2022, Channel mapping Glen Canyon Dam to Lees Ferry in Glen Canyon National Recreation Area—Data: U.S. Geological Survey data release, https://doi.org/10.5066/P98GFP93.

ISSN 2331-1258 (online)

Contents

Figures

Tables

Conversion Factors

U.S. customary units to International System of Units

Multiply	By	To obtain
	Length	
mile (mi)	1.609	kilometer (km)
	Flow rate	
cubic foot per second (ft^3/s)	0.02832	cubic meter per second (m^3/s)

International System of Units to U.S. customary units

Multiply	By	To obtain
	Length	
centimeter (cm)	0.3937	inch (in.)
millimeter (mm)	0.03937	inch (in.)
meter (m)	3.281	foot (ft)
	Area	
square kilometer (m^2)	0.386102	square mile (mi^2)
	Sound velocity	
meter per second (m/s)	3.281	foot per second (ft/s)

Datums

Vertical coordinate information is referenced to the Geodetic Reference System 1980 ellipsoid defined by the 2011 adjustment of the North American Datum of 1983 (NAD 83[2011]).

Horizontal coordinate information is referenced to NAD 83(2011) and projected to the State Plane Coordinate System of 1983, Arizona Central Zone, in meters.

Elevation, as used in this report, refers to distance above the Geodetic Reference System 1980 ellipsoid defined by NAD 83(2011).

Abbreviations

ASCII	American Standard Code for Information Interchange
DEM	digital elevation model
FIS	fuzzy inference system
GLCA	Glen Canyon National Recreation Area
GNSS	Global Navigation Satellite System
HFE	high-flow experiment
INS	inertial navigation system
NAD 83(2011)	2011 national adjustment of the North American Datum of 1983
RM	river mile
TIN	triangular irregular network
USGS	U.S. Geological Survey

Channel Mapping of the Colorado River from Glen Canyon Dam to Lees Ferry in Glen Canyon National Recreation Area, Arizona

By Matt Kaplinski,[1] Joseph E. Hazel, Jr.,[1] Paul E. Grams,[2] Tom Gushue,[2] Daniel D. Buscombe,[3] and Keith Kohl[2]

Abstract

Bathymetric and topographic data were collected from May 2013 to February 2016 along the 15.84-mile reach of the Colorado River spanning from Glen Canyon Dam to Lees Ferry in Glen Canyon National Recreation Area, Arizona. Channel bathymetry was mapped using multibeam and singlebeam echo sounders; subaerial topography was mapped using a combination of ground-based total stations and aerial photogrammetry. These data were combined to produce a digital elevation model (DEM), spatially variable estimates of DEM uncertainty, and bed-substrate distribution maps. This project is part of a larger effort to monitor the status and trends of sand storage along the Colorado River in Glen Canyon National Recreation Area and Grand Canyon National Park. This report documents the study methodologies (survey methods and post-processing procedures, DEM production and uncertainty assessment, and bed-substrate classification) and presents the resulting datasets.

Introduction

Fluvial geomorphologists and ecologists rely on topographic data to study the landscapes and physical habitats of rivers. Topographic data are used to calculate hydraulic geometry, create hydraulic models, and (where there have been repeated topographic surveys) measure geomorphic change. Historically, river topography was measured along transects, or cross sections (Williams, 1978; Graf and others, 1995; Liu and others, 2019). Technological developments over the past two decades (such as portable shallow-water multibeam sonar systems and high-resolution image processing) have enabled the development of digital elevation models (DEMs) that accurately characterize entire river valleys at the meter or sub-meter scale. DEMs of these scales have become the primary building blocks for characterizing geomorphic processes and ecological functions by providing valuable inputs to hydraulic and ecosystem modeling efforts. This study combines multiple spatial data products into a single 1-meter scale DEM with spatially distributed uncertainty and classification of bed substrate of the Colorado River from Glen Canyon Dam to Lees Ferry in Glen Canyon, Arizona.

The U.S. Bureau of Reclamation completed the construction of Glen Canyon Dam in 1963. The dam and its operations have since drastically changed the flow, sediment, and temperature regimes of the Colorado River—and consequently the geomorphology and ecology of the river corridor—downstream from the dam (U.S. Department of Interior, 1995). Dam operations have altered seasonal flow variability by eliminating long duration spring snowmelt floods; raised the median discharge during the summer, fall, and winter; and introduced daily flow fluctuations to generate hydropower (Topping and others, 2003). Additionally, the dam blocks the delivery of sediment from the upstream watershed, and because the dam's penstocks are well below the surface of Lake Powell, water released from the dam is clear and cold (with an average temperature of 8 degrees Celsius; Webb and others, 1999).

Downstream from Glen Canyon Dam, the geomorphic and ecologic changes caused by the dam to Glen Canyon are extensive. Changes in flow and sediment delivery have caused the channel to incise, narrow, and armor, and the once sand-bedded channel is now primarily gravel-bedded and immobile under most flow releases (Pemberton, 1976; Grams and others, 2007). Along the river banks, alluvial sand and gravel deposits—no longer regularly inundated—are separated from the functional floodplain of the river and colonized by plants. These deposits also contain valuable archeological remains that are susceptible to erosion from localized precipitation runoff. Ecologically, the cold, clear water has led to the proliferation of native and non-native aquatic vegetation and the replacement of native fish communities by introduced trout (Sankey and others, 2015; Kennedy and others, 2016; Korman and others, 2017; Ralston and others, 2017).

Because of these changes, the Colorado River corridor downstream from the dam has become the focus of several research projects that address a range of environmental and recreational issues. All of these projects stand to benefit from a complete topographic map of the river corridor. This

[1]Northern Arizona University

[2]U.S. Geological Survey

[3]Marda Science LLC

report describes the production of a DEM from topographic and bathymetric surveys conducted in the study area from 2013 to 2016, the procedures used to estimate the uncertainty associated with the DEM, and the production of bed-substrate distribution maps. The resulting DEM and bed-substrate distribution maps will provide insight into the geomorphic framework of the river corridor and input to flow modeling efforts, improve the understanding of aquatic and riparian habitats for environmental monitoring and research, and provide the recreational community a complete topographic map of the Colorado River through Glen Canyon.

Study Area, Place Names, and Units

The study area (also referred to in this report as the "Glen Canyon reach" or "study reach") is the 15.84-mile (mi) reach of the Colorado River corridor spanning from Glen Canyon Dam to Lees Ferry in Glen Canyon National Recreation Area (GLCA), Arizona (fig. 1). Locations discussed in this report are referenced by the U.S. Geological Survey (USGS) Grand Canyon Monitoring and Research Center river mile (RM) system of Gushue (2019)—that is, by their distance downstream or upstream from Lees Ferry as measured in miles along the channel centerline. Locations downstream from Lees Ferry are denoted by positive mileages, and locations upstream from Lees Ferry are denoted by negative mileages. For example, Glen Canyon Dam is located 15.84 mi upstream from Lees Ferry (RM 0) and is denoted as RM -15.84, whereas the mouth of the Paria River is located 1 mi downstream from Lees Ferry and denoted as RM 1 (fig. 1). Units of streamflow are reported in cubic feet per second (ft^3/s).

In order to integrate spatial datasets from different sources in a composite DEM, all topographic and bathymetric data were projected to the Arizona Central Zone of the State Plane Coordinate System of 1983 in meters (Stem, 1989) and constrained to the 2011 national adjustment of the North American Datum of 1983 (NAD 83[2011]). Elevations in this report refer to distances above the Geodetic Reference System 1980 ellipsoid defined by NAD 83(2011).

Data Collection and Processing

The following sections describe the methods used to survey and process the data collected in Glen Canyon between May 2013 and February 2016. Whereas channel mapping surveys downstream from Lees Ferry require multi-week wilderness river trips to collect data, the relatively easy access provided by the Lees Ferry boat ramp to the Glen Canyon reach upstream from Lees Ferry allowed us

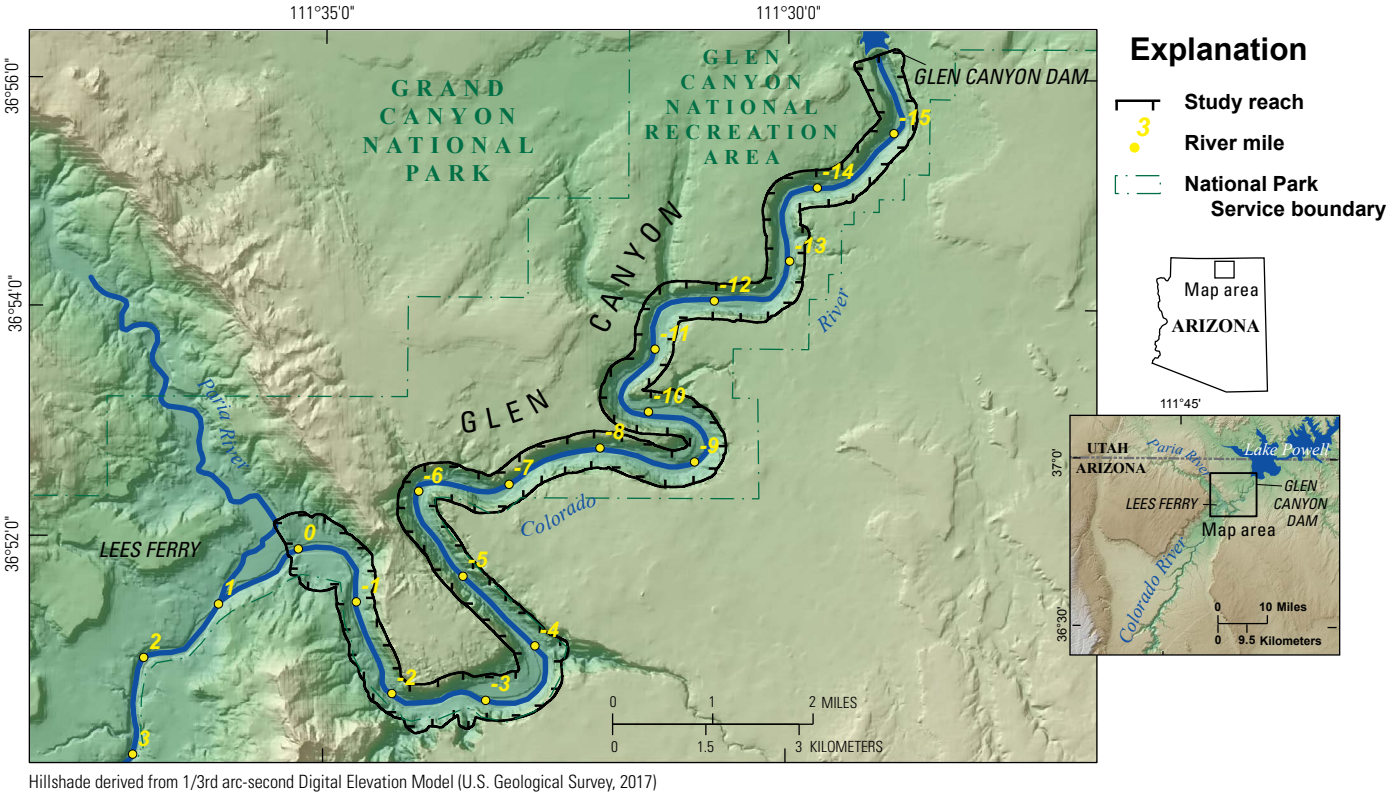

Hillshade derived from 1/3rd arc-second Digital Elevation Model (U.S. Geological Survey, 2017)

Figure 1. Map showing location of the study reach, Glen Canyon National Recreation Area, Arizona. River mileage from Gushue (2019).

to conduct the surveys on several 1- to 7-day trips within a 16-month period. The Glen Canyon reach is relatively shallow, which makes full-channel multibeam surveys challenging (if not impossible) during normal flow levels (8,000 ft^3/s to 18,000 ft^3/s). To work around this issue, we conducted multibeam sonar surveys during the November 2014 high-flow experiment (HFE) when flows were approximately 38,000 ft^3/s in order to take advantage of the greater water depths. For topographic data at a higher elevation than bathymetric survey coverage, we used a 1-m resolution digital surface model that was photogrammetrically-derived from aerial photography collected in 2013 (Durning and others, 2016a, 2016b) and ground-based total station surveys. Surveys using ground-based total stations and singlebeam sonar were conducted in February 2015, October 2015, and February 2016. Flows during total station and singlebeam data collection fluctuated daily between approximately 18,000 ft^3/s and 6,500 ft^3/s. The multibeam sonar dataset also contains georeferenced backscatter and auxiliary sonar information that was used to classify bed substrate in those areas mapped by multibeam sonar at the same resolution as the bathymetry. Grams and others (2007) concluded that the channel bed and banks in Glen Canyon are stable and unlikely to be mobilized by Glen Canyon Dam operations, and we assume that the channel bed was immobile during the data collection period. Parts of the channel bed, such as sandbars and other patches of sand or small gravel, may have been partially mobilized during the November 2014 HFE. However, because we conducted singlebeam and total station surveys after the HFE, any changes that may have occurred were captured by the surveys. Results from the surveys are integrated in a geographic information system to construct the DEM, uncertainty surfaces, and bed-substrate classification maps.

Geodetic Control Network

A network of geodetic control benchmarks was established along the canyon rim and the river corridor. Coordinates of benchmarks along the north and south rims were computed through multiple, independent static Global Navigation Satellite System (GNSS) observations using the procedures described by Zilkoski and others (1997) and published in the National Spatial Reference System using National Geodetic Survey protocols (Doyle, 1994). The control network for topographic and bathymetric mapping along the Colorado River corridor includes both GNSS and total station measurements. Terrestrial total station measurements to and from monuments along the river corridor have been constrained to the globally derived GNSS positions using the methods of least squares (Zilkoski and others, 1997). Network accuracy of the GNSS-derived benchmarks in relation to the NAD 83(2011) ellipsoid was 0.004 meter (m) horizontal and 0.029 m vertical at 68 percent confidence, and 0.007 m horizontal and 0.052 m vertical at 95 percent confidence. Network accuracy of the total station benchmarks was 0.015 m horizontal and 0.027 m vertical at 68 percent confidence, and 0.033 m horizontal and 0.052 m vertical at 95 percent confidence. Within the study area, the control network comprises 53 benchmarks, 43 of which were occupied with total stations for this study.

Conventional Total Station Surveys

Total station surveys were used to collect measurements for a variety of purposes. The primary purpose of the total station surveys was to collect ground points used for defining riverbank topography. In addition, total station surveys were used to position temporary benchmarks for line-of-sight multibeam and singlebeam surveys, quantify the spatial accuracy of the digital surface model dataset, and record measurements between benchmarks that provide information for refinement of the geodetic control network.

Total station surveys use manually operated electronic total stations (such as Topcon GTS-313, GPT-2003, GTS-233, or similar models). An operator plumbs the instrument on a tripod over a control network monument and orients its direction by referencing a tripod and prism over a second known benchmark, typically at a distance of 600 m or less. Horizontal and zenith angles (1-arcsecond precision; 1/3,600 degree) and slope distances (1-millimeter precision) to the backsight are recorded in both forward and reverse faces of the instrument. Resulting coordinates are computed and field results are immediately compared to the geodetic network coordinates. This initial quality control (1) ensures that the instrument is able to repeatedly and precisely index a target, (2) validates proper collimation of the instrument and that the crosshairs are level and plumb, (3) records results of the instrument collimation, and (4) verifies that the instrument operator is referencing correct benchmark coordinates.

The local or relative accuracy of total station surveys is determined by the ability to match control network results with in-field measurements. Statistical analysis of these data shows that about 68 percent of the field measurements are within 0.011 m horizontal and 0.012 m vertical of GNSS results, and 95 percent of these measurements are within 0.031 m horizontal and 0.034 m vertical of GNSS results.

Topographic measurements are made by sighting to a reflecting prism target mounted on portable survey rods operated by one or more field assistants (fig. 2). Total station surveys capture sandbars, water-surface elevations, and shallow (for example, less than 1 m) offshore locations. Topographic break lines are collected along continuous features such as dune crests, terraces, and the water's edge along the shoreline; and these sharp breaks in topography and (or) linear features are linked during surveying to create break lines for proper terrain modelling.

Bathymetric Surveys

Bathymetric surveys were collected using both multibeam and singlebeam sonar systems deployed on motorized rafts (fig. 3). The multibeam mapping system

was mounted on the RV *Greg Sponenbergh*, a 7-m inflatable pontoon (snout) raft powered by a 50-horsepower 4-stroke outboard motor (fig. 3*A*). The singlebeam mapping system was mounted on the RV *Frank Protiva*, a 5-m inflatable pontoon (mini-snout) raft, also powered by a 50-horsepower 4-stroke outboard motor (fig. 3*B*).

The multibeam system used a 455-kilohertz (kHz) RESON Seabat 7125 multibeam echo sounder mounted on the bow of the survey vessel frame to collect bed surface elevation and acoustic backscatter data. A sound velocity probe (RESON SV-71) is attached to the echo sounder head to continuously measure the speed of sound near the water surface. Periodic casts of a sound velocity probe show that the water column is very well mixed, varying only by about 0.2 meter per second (m/s) from the sound velocity measured at the surface (Buscombe and others, 2014a). An IxSea Hydrins inertial navigation system was used to collect roll, pitch, and heading information. The singlebeam system used an Odom CV-100 singlebeam echo sounder with a 200-kHz transducer mounted off the starboard bow of the survey vessel. Both bathymetry systems used a line-of-sight, range-azimuth navigation system (Kaplinski and others, 2009, 2014, 2017). The range-azimuth system uses a 1-second robotic total station (Trimble SPS930) located on a control network benchmark to track the position and elevation of the survey vessel at a maximum range from the instrument of about 500 m. The

Figure 2. Photographs of survey crew members conducting total station surveys along the Colorado River, Arizona. *A*, Crew member using total station established over geodetic control benchmark. *B*, Survey crew members using stadia rod and prism to survey edge of water. Photographs by Joseph E. Hazel, Jr., Northern Arizona University.

Figure 3. Photographs showing sonar survey vessels used in this study, in Grand Canyon National Park area, Arizona. *A*, Multibeam survey vessel RV Greg Sponenbergh. *B*, Singlebeam survey vessel RV Frank Protiva. Photographs by Joseph E. Hazel, Jr., Northern Arizona University.

raw positioning information (slope distance, horizontal and vertical angles) is referenced to the benchmark location and transmitted to the survey vessel by radio modem at a rate of 20 hertz. The measured depths are subtracted from the elevation of the transducer to derive bed elevations. The accuracy of the Trimble® SPS930 to a target 100 m from the instrument moving at 1 m/s is specified by the manufacturer as ±0.002 m for horizontal, vertical, and slope distance measurements. HYPACK software was used to collect and process survey data.

The general strategy for surveying was to first collect the multibeam dataset and then conduct singlebeam surveys in areas not covered by multibeam data. Before multibeam data collection, the system was calibrated by conducting a patch test that identifies angular offsets between system components (U.S. Army Corps of Engineers, 2013). Results from the patch test are used to remove any systematic bias introduced by mounting the system components. Whenever possible, we restricted multibeam surveys to depths of about 2 m beneath the sonar head in order to minimize the risk of damage to the sonar transducer. Multibeam surveys were collected without planned line files and used online visual display of coverage maps to achieve a 50 percent overlap in coverage. Given the time-sensitive nature of the surveys (attempting to finish multibeam mapping during the HFE), the percentage of overlap in shallow areas was approximately 1–20 percent. Preliminary maps of the multibeam surveys were generated to define the extent of multibeam coverage and determine the extent of singlebeam mapping necessary to ensure continuous coverage of the survey area. The singlebeam system was used to survey the entire channel in a few particularly shallow (less than about 2 m in depth) areas within the study reach. For these full-channel singlebeam surveys, data were collected along planned lines with 15-m spacing in the cross-stream direction and about 15-m spacing in the stream-wise direction.

Upon completion of the surveys, bathymetric data were processed and edited to correct any survey errors and to identify and remove erroneous soundings. The editing of bathymetric data, particularly multibeam soundings, requires skilled judgement and was the most time-consuming aspect of data processing. Sonar data collected in shallow, fast-moving rivers are inherently noisy because of a combination of steep slopes, topographic complexity, side-lobe effects, multipath effects, water-column targets (air bubble, suspended particles, fish, and so on), and ambient high-frequency noise. Identification and removal of soundings that do not represent the channel bed require that all soundings are visually inspected and manually edited. After the multibeam soundings were edited, they were converted to grid values by calculating the median elevation of soundings within 0.25-m square grid cells and then output as human-readable, or American Standard Code for Information Interchange (ASCII), format files. Singlebeam data were filtered to only include one median elevation per meter along each survey trackline and were output as ASCII text files. The 0.25-m and 1-m decimated datasets from both the multibeam and singlebeam systems were used to construct the bathymetric parts of the DEM.

Digital Surface Model from 2013 Aerial Photography

In May 2013, the USGS Grand Canyon Monitoring and Research Center acquired multispectral high-resolution aerial imagery for the Colorado River in the Grand Canyon, Arizona (Durning and others, 2016a). The imagery, which consist of four color bands (blue, green, red, and near-infrared) with a ground resolution of 20 centimeters, are available in the data release by Durning and others (2016b). A Leica ADS80 SH52 push-broom multispectral sensor was used during image collection. The river corridor was flown using 5 or 6 parallel flight lines per river segment with adjacent flight lines overlapping 50 percent. Flow releases from GCD were held to approximately 8,000 ft^3/s to provide a stable and consistent water surface level in all imagery.

Each stereo-image composite was processed by the data-collection contractor. The ADS80 collections processing steps consisted of (1) determining tie points between all flightline images to determine image relative position, (2) determining the absolute position of the flightline images using solutions from the airborne inertial motion system and the ground GNSS base stations, (3) incorporating the ground-control-panel data to produce a final aerotriangulation block adjustment for each flightline image dataset, and (4) using the Pixel Factory photogrammetric software to derive the digital surface model from the imagery. The final digital surface model data were delivered with a 1-m cell resolution.

The photogrammetric process does not discriminate between the ground surface and vegetation. As a result, the final digital surface model dataset contains points that, in densely vegetated areas, represent the top of vegetation rather than the ground surface. Therefore, digital surface model points within vegetated shoreline areas were deleted by masking points from the digital surface model dataset that lie within the riparian vegetation classification map developed by Durning and others (2018).

Bed-Substrate Classification

Backscatter data from the multibeam sonar data were processed using the spectral analysis methods of Buscombe and others (2014a, 2014b, 2017) to produce maps of surface sediment type and vegetation density. The backscatter magnitude is computed per beam by balancing the active sonar equation, which accounts for losses in acoustic energy caused by spherical spreading, attenuation by water and sediment, and the physical footprint of the beam. Because of the high water clarity in the Glen Canyon reach, there is an abundance of submerged aquatic vegetation. Buscombe and others (2017) devised a classification system that discriminates between the following four substrate types: dense vegetation, denoted as “V”; sparsely vegetated sand and (or) gravel, denoted as “vSG”; unvegetated gravel and (or) cobble, denoted as “Gc”; and unvegetated cobble, boulder, and (or) bedrock, denoted as “cBR.” These classifications are continuous in space at 0.25 by 0.25 m grid cell resolution. The process uses

backscatter statistics related to georeferenced underwater video observations of the bed. Vegetated substrates were classified using a simple and qualitative visual estimation: if the substrate was completely covered in vegetation, it was classified as densely vegetated, whereas if the substrate was partially covered with vegetation, it was classified as sparsely vegetated. The variance of the power spectrum and the intercept and slope from a power-law spectral form (termed the spectral strength and exponent, respectively) are used to discriminate between substrate types using a random forest classifier, which is a machine-learning technique that fits decision-tree classifiers on various subsamples of the data and uses averaging to improve the predictive accuracy. Buscombe and others (2017) showed that substrates classified using these methods in the Glen Canyon reach were accurate to within 70 to 100 percent of photographic ground-truth stations.

Digital Elevation Model

The total station, digital surface model, multibeam, and singlebeam data points were combined to construct a DEM of the channel bed, banks, and surrounding cliffs for the entire study reach in a geographic information system (fig. 4; Kaplinski and others, 2014; Kaplinski and others, 2017). Where bathymetry data points overlapped, priority was given to the higher density multibeam data points. This was accomplished by creating a polygon surrounding the multibeam point data that was used to clip the singlebeam coverage to erase singlebeam points in areas of overlap. The remaining digital surface model, total station, multibeam, and singlebeam points were then used to create a triangular irregular network (TIN) model from the point data using a Delaunay triangulation (Peuker and others, 1978). Break lines were incorporated in the TIN model along morphological grade-breaks and other features to accurately represent the topographic surface (see section "Conventional Total Station Surveys"). The TIN model was edited to ensure that the model best represented the topographic surface and eliminated excessive interpolation. Triangular facets along the outer edge of the TIN model that were greater than about 10 m were eliminated. Contour and shaded relief maps were used to inspect the TIN model surface; any errors detected during data collection (such as improper rod height coding or crossing break lines) were edited and additional break lines were added to accurately depict changes in grade. The edited TIN was then used to generate the 1-m resolution raster DEM from the TIN model using linear interpolation (fig. 4).

Digital Elevation Model Uncertainty

Accounting for elevation uncertainty is a critical part of monitoring studies that compare sequential digital elevation models to detect spatial patterns and volumes of morphological change (Brasington and others, 2003; Lane and others, 2003; Wheaton and others, 2010). DEM elevation uncertainty is affected by many factors, including measurement errors associated with the survey methods used, topographic complexity, point density, and interpolation method (Lane, 1998; Heritage and Large, 2009; Wheaton and others, 2010). We first estimated the measurement uncertainty using quality control checks for each survey method, then used derivative products from the topographic data itself to construct a spatially variable elevation uncertainty model for the DEM using fuzzy inference system (FIS) modeling.

Measurement Uncertainty

Measurement uncertainty estimates define the minimum level of uncertainty, or the lowest uncertainty attainable using the survey equipment specific to each data-collection type. For each survey type (digital surface model, total station, multibeam, and singlebeam), we compared survey data to the elevation of check points or reference surfaces (fig. 5) to derive estimates of measurement uncertainty. The results of this analysis are presented using a standard set of statistical parameters: mean, median, mean absolute error, 95 percent root mean square error, standard deviation, kurtosis, skewness, and count (or number of samples; table 1). We use the mean absolute error value as the measurement uncertainty for each survey type (Willmott and Matsuura, 2005).

Digital surface model measurement uncertainty was estimated by comparing digital surface model-derived elevations with 986 total station points. The total station points were either collected specifically for digital surface model testing by selecting areas that were located on bedrock surfaces with low slope (less than 5 degrees, as estimated in the field) and no vegetation, or by selecting points that were located on surfaces assumed to have not changed in elevation (gravel bars, bedrock) and at least two meters from vegetation. The results of the digital surface model measurement uncertainty estimates are shown in figure 6 and table 2.

Multibeam measurement uncertainty was estimated by conducting a performance test. A performance test compares a "check line" dataset with a "reference surface" dataset constructed from narrowly spaced multibeam data (U.S. Army Corps of Engineers, 2013). The reference surface was developed over a relatively flat area with depths of about 6 m. A 0.25 by 0.25 m grid reference surface was constructed by collecting data from multiple passes over a small patch of the riverbed. Soundings from all passes were filtered to only use soundings with a beam angle of less than 45 degrees, and the median elevation of the soundings in each cell was assigned as the cell elevation. Soundings from a survey line using all beam angles (0 to 70 degrees) passing through the reference surface were compared to the coincident cell elevation of the reference surface. The results of the multibeam measurement uncertainty estimates are shown in figure 7 and table 3.

The measurement uncertainty for singlebeam surveys was also estimated using a performance test in the same area used for the multibeam test. This was accomplished by collecting several singlebeam lines over the reference surface developed

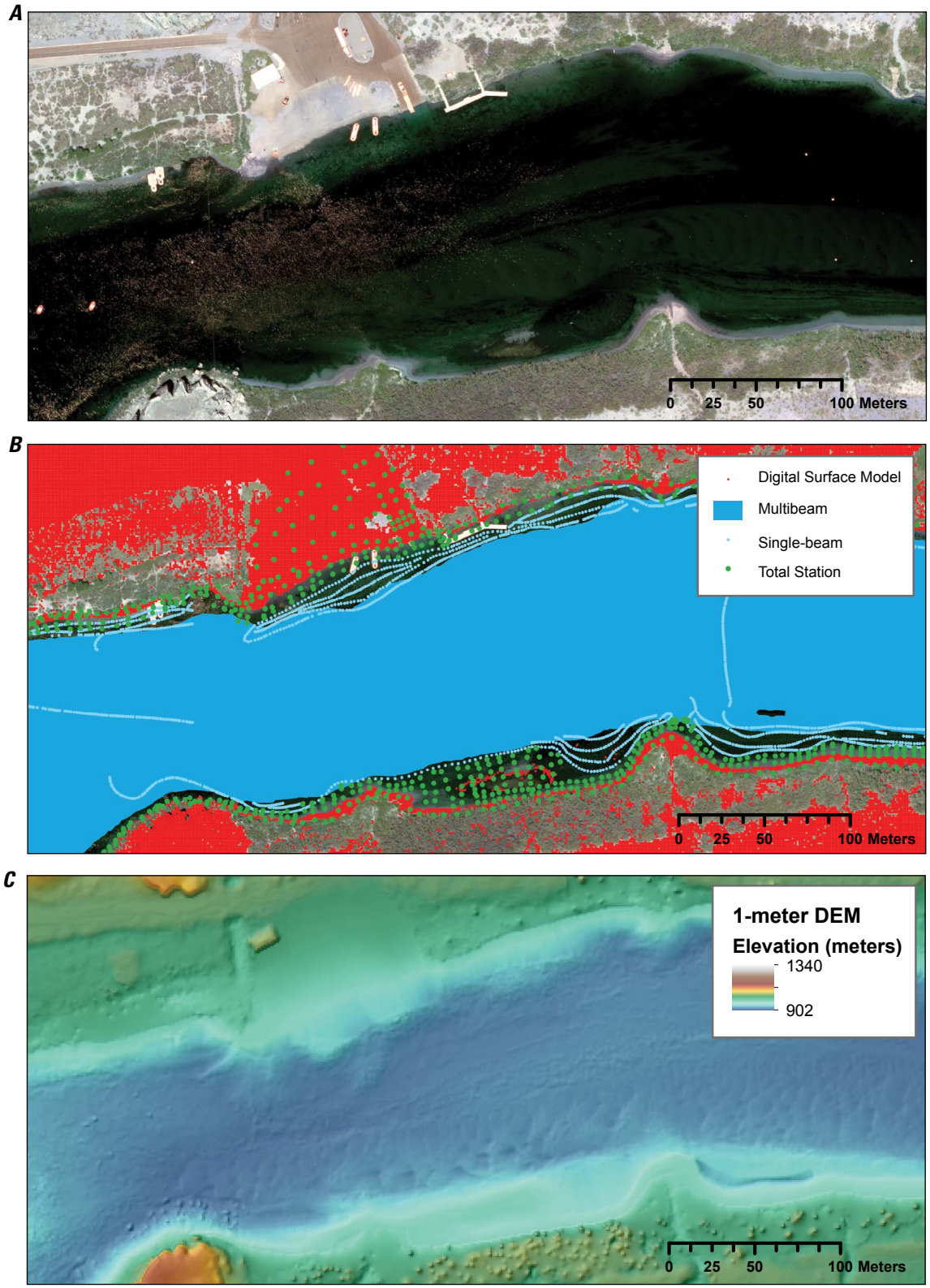

Figure 4. Maps of the Lees Ferry area showing examples of the types and spatial distribution of data used to develop the digital elevation model (DEM) for the study reach, Glen Canyon National Recreation Area, Arizona. *A*, Orthophotograph (0.2-meter resolution) collected in May 2013 showing Colorado River near Lees Ferry. *B*, Survey data points from digital surface model, multibeam, singlebeam, and total station surveys (base imagery is same as that shown in *A*). *C*, 1-meter DEM generated from triangular irregular network model.

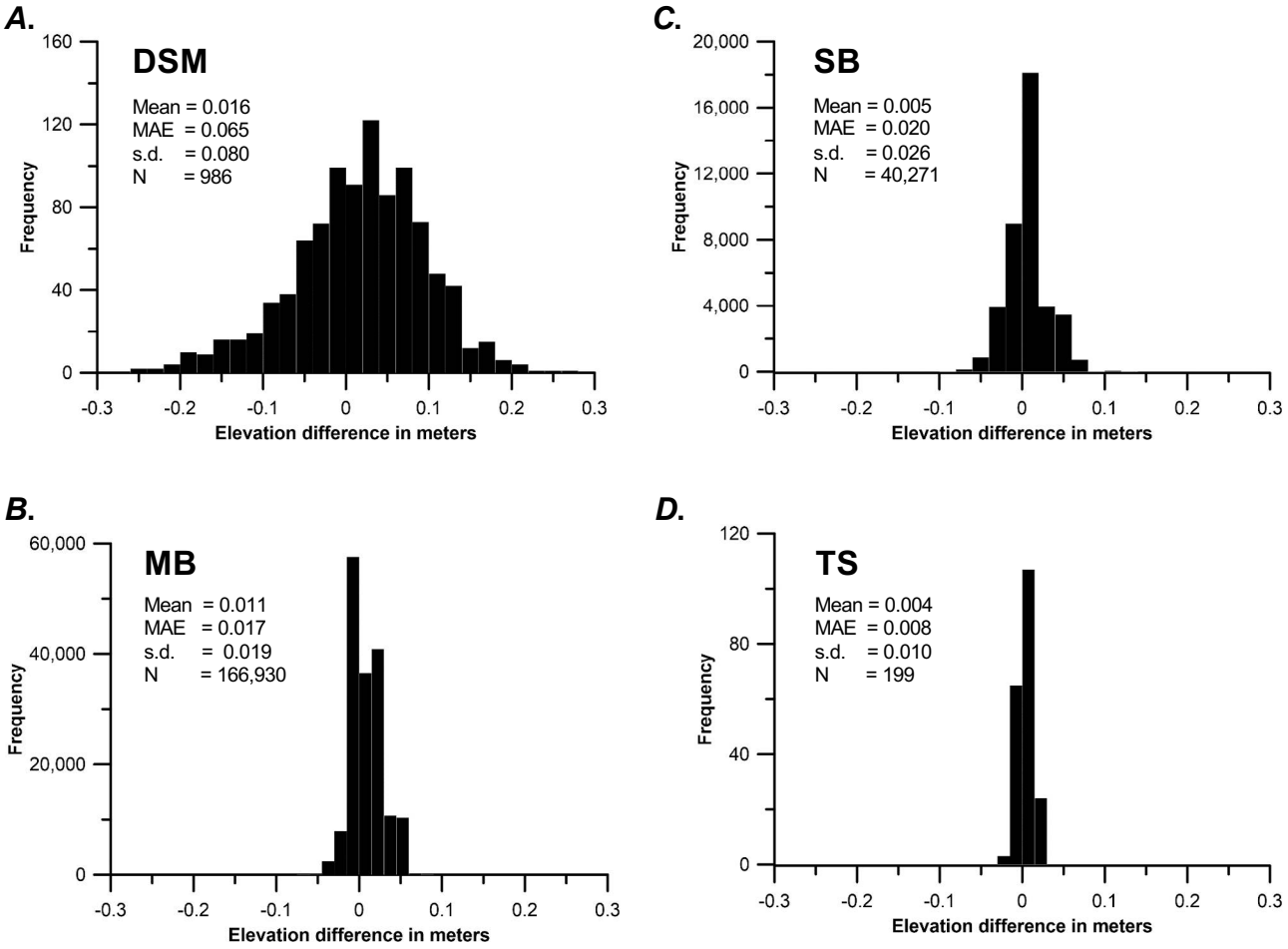

Figure 5. Histograms of survey measurement uncertainty for each survey type. *A*, Histogram of elevation difference between digital surface model (DSM) and total station (TS) checkpoints. *B*, Histogram of elevation difference between multibeam (MB) reference surface and MB check lines. *C*, Histogram of elevation difference between singlebeam (SB) check lines and MB reference surface. *D*, Histogram of elevation difference between TS observations and geodetic control benchmarks. Statistics computed from measurement uncertainty analysis of elevation difference between survey type and test measurements. Mean, mean absolute error (MAE), and standard deviation (SD) in meters; count is number of samples.

Table 1. Summary of statistics of measurement uncertainty for each survey type.

[Mean, median, MAE, 95% RMSE, and standard deviation are given in meters. DSM, digital surface model; MB, multibeam; SB, singlebeam; TS, total station; MAE, mean absolute error; RMSE, root mean square error]

Statistic[1]	DSM	MB	SB	TS
mean	0.016	0.011	0.005	0.004
median	0.023	0.01	0.01	0.004
MAE	0.065	0.017	0.020	0.008
95% RMSE	0.161	0.038	0.050	0.019
standard deviation	0.080	0.019	0.026	0.010
kurtosis	0.401	-0.045	0.383	-0.217
skewness	-0.379	0.380	0.014	-0.067
count	986	166,930	40,271	199

[1]Statistics computed from measurement uncertainty analysis of elevation difference between survey data and test measurements.

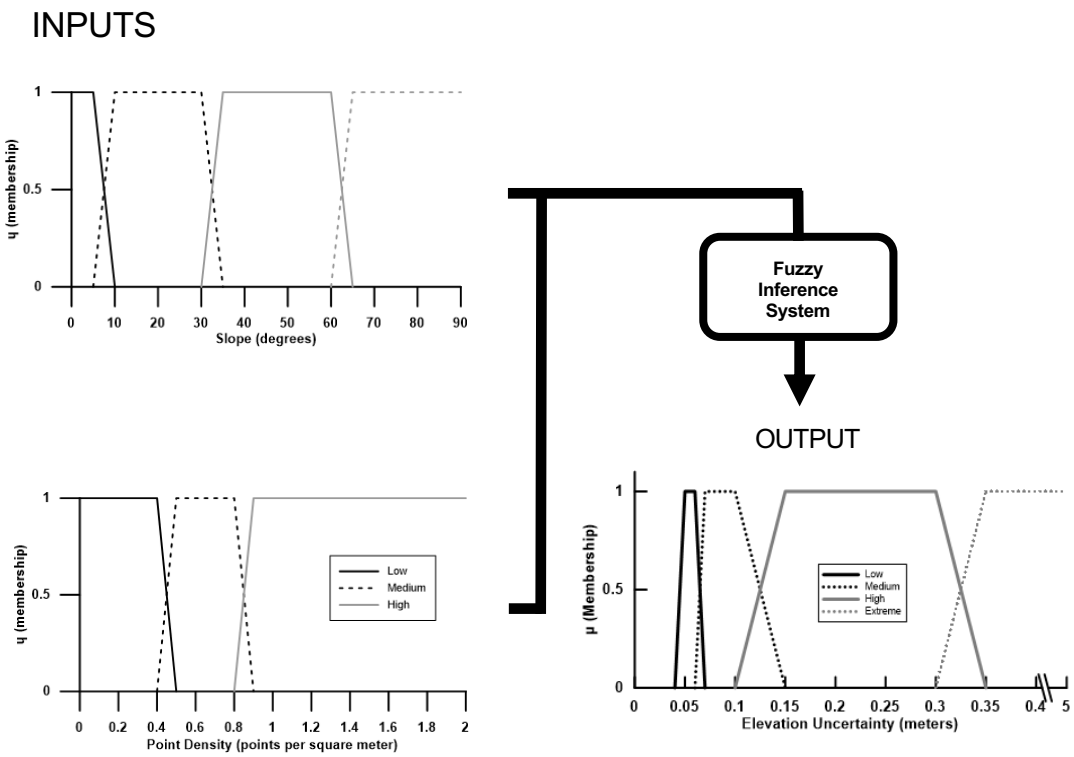

Figure 6. Diagram of fuzzy inference system model for digital surface model survey areas showing input and output membership functions. Inputs are slope and point density. Output is elevation uncertainty. Note the variable x-axis break in output function.

Table 2. Two-input fuzzy inference system ruleset for digital surface model surveys.

Rule	Inputs		Output (meters)
	Slope (degrees)	Point density (points per square meter)	
1	Low	Low	High
2	Low	Medium	Medium
3	Low	High	Low
4	Medium	Low	High
5	Medium	Medium	Medium
6	Medium	High	Low
7	High	Low	High
8	High	Medium	Medium
9	High	High	Medium
10	Extreme	Low	Extreme
11	Extreme	Medium	Extreme
12	Extreme	High	Extreme

for the multibeam performance test. The difference in elevation between the singlebeam points and reference surface was used to provide an estimate of singlebeam measurement uncertainty. The results of the singlebeam measurement uncertainty estimates are shown in figure 8 and table 4.

The measurement uncertainty associated with the total station surveys was estimated by comparing the elevation of total station observations to geodetic control benchmarks. For the comparison, an extendable survey rod was targeted by a total station at each extension whilst plumbed over a control point, and the difference in elevation between the total station observation and control point elevation was used to estimate the measurement uncertainty. The results of the total station measurement uncertainty estimates are shown in figure 9 and table 5.

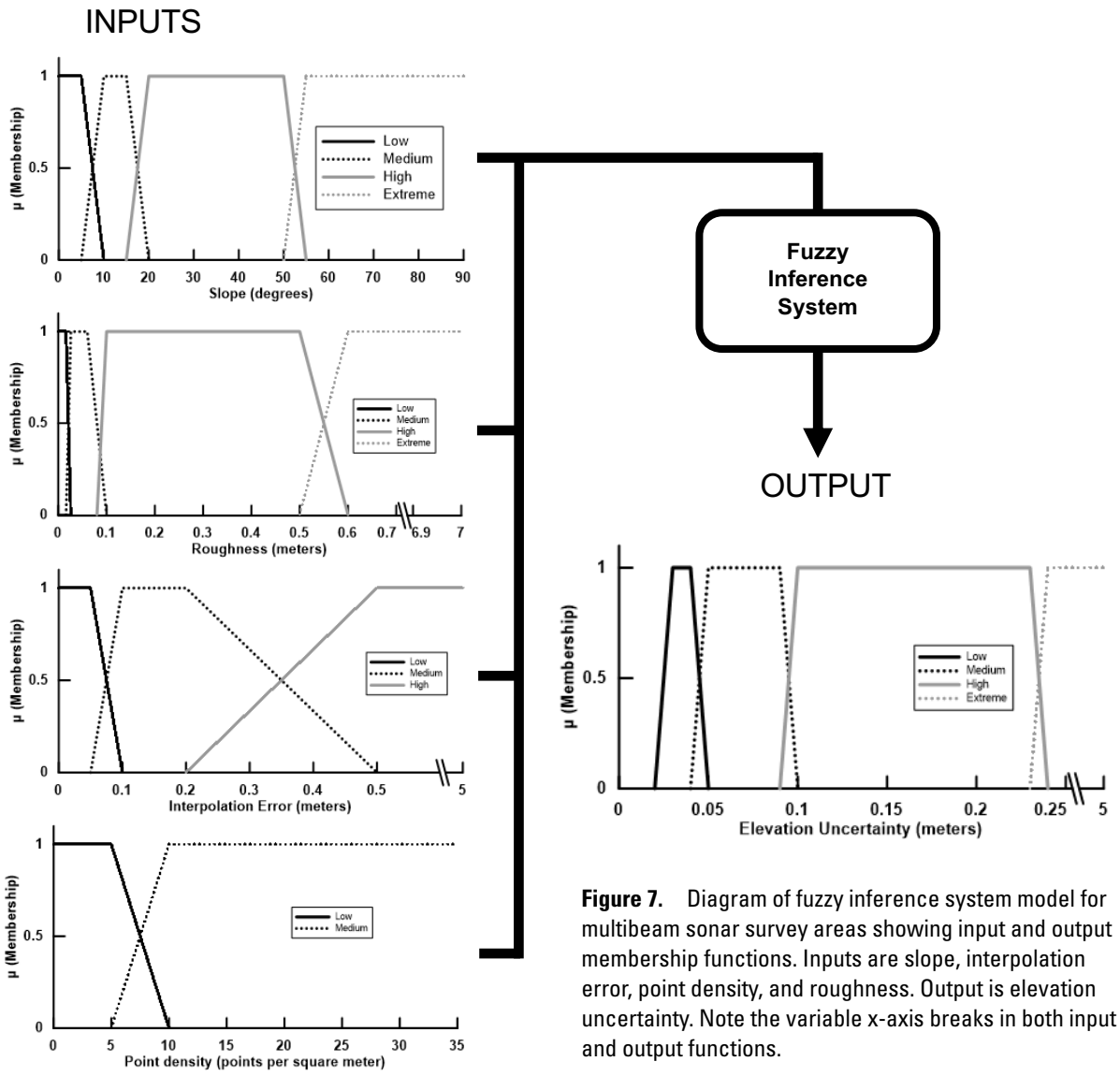

Figure 7. Diagram of fuzzy inference system model for multibeam sonar survey areas showing input and output membership functions. Inputs are slope, interpolation error, point density, and roughness. Output is elevation uncertainty. Note the variable x-axis breaks in both input and output functions.

Table 3. Four-input fuzzy inference system ruleset for multibeam sonar surveys.

Rule	Inputs				Output (meters)
	Slope (degrees)	Roughness (meters)	Interpolation (meters)	Point density (points per square meter)	
1	Low	Low	Low	Low	Medium
2	Low	Low	Low	High	Low
3	Low	Medium	Low	Low	Medium
4	Low	Medium	Low	High	Medium
5	Low	High	Low	Low	High
6	Low	High	Low	High	Medium
7	Low	Extreme	Low	Low	High
8	Low	Extreme	Low	High	High
9	Low	Low	Medium	Low	Medium
10	Low	Low	Medium	High	Low
11	Low	Medium	Medium	Low	Medium
12	Low	Medium	Medium	High	Medium

Table 3. Four-input fuzzy inference system ruleset for multibeam sonar surveys.—Continued

Rule	Inputs				Output (meters)
	Slope (degrees)	Roughness (meters)	Interpolation (meters)	Point density (points per square meter)	
13	Low	High	Medium	Low	High
14	Low	High	Medium	High	High
15	Low	Extreme	Medium	Low	High
16	Low	Extreme	Medium	High	High
17	Low	Low	High	Low	Medium
18	Low	Low	High	High	Medium
19	Low	Medium	High	Low	Medium
20	Low	Medium	High	High	Medium
21	Low	High	High	Low	High
22	Low	High	High	High	High
23	Low	Extreme	High	Low	High
24	Low	Extreme	High	High	High
25	Medium	Low	Low	Low	Medium
26	Medium	Low	Low	High	Low
27	Medium	Medium	Low	Low	Medium
28	Medium	Medium	Low	High	Medium
29	Medium	High	Low	Low	Medium
30	Medium	High	Low	High	Medium
31	Medium	Extreme	Low	Low	High
32	Medium	Extreme	Low	High	High
33	Medium	Low	Medium	Low	Medium
34	Medium	Low	Medium	High	Medium
35	Medium	Medium	Medium	Low	Medium
36	Medium	Medium	Medium	High	Medium
37	Medium	High	Medium	Low	High
38	Medium	High	Medium	High	High
39	Medium	Extreme	Medium	Low	High
40	Medium	Extreme	Medium	High	High
41	Medium	Low	High	Low	High
42	Medium	Low	High	High	High
43	Medium	Medium	High	Low	High
44	Medium	Medium	High	High	High
45	Medium	High	High	Low	High
46	Medium	High	High	High	High
47	Medium	Extreme	High	Low	High
48	Medium	Extreme	High	High	High
49	High	Low	Low	Low	Medium
50	High	Low	Low	High	Low
51	High	Medium	Low	Low	Medium
52	High	Medium	Low	High	Medium
53	High	High	Low	Low	High
54	High	High	Low	High	High
55	High	Extreme	Low	Low	High

Table 3. Four-input fuzzy inference system ruleset for multibeam sonar surveys.—Continued

Rule	Inputs				Output (meters)
	Slope (degrees)	Roughness (meters)	Interpolation (meters)	Point density (points per square meter)	
56	High	Extreme	Low	High	High
57	High	Low	Medium	Low	Medium
58	High	Low	Medium	High	Medium
59	High	Medium	Medium	Low	Medium
60	High	Medium	Medium	High	Medium
61	High	High	Medium	Low	High
62	High	High	Medium	High	High
63	High	Extreme	Medium	Low	High
64	High	Extreme	Medium	High	High
65	High	Low	High	Low	High
66	High	Low	High	High	High
67	High	Medium	High	Low	High
68	High	Medium	High	High	High
69	High	High	High	Low	High
70	High	High	High	High	High
71	High	Extreme	High	Low	High
72	High	Extreme	High	High	High
73	Extreme	Low	Low	Low	Medium
74	Extreme	Low	Low	High	Low
75	Extreme	Medium	Low	Low	Medium
76	Extreme	Medium	Low	High	Medium
77	Extreme	High	Low	Low	High
78	Extreme	High	Low	High	High
79	Extreme	Extreme	Low	Low	Extreme
80	Extreme	Extreme	Low	High	Extreme
81	Extreme	Low	Medium	Low	Medium
82	Extreme	Low	Medium	High	Medium
83	Extreme	Medium	Medium	Low	Medium
84	Extreme	Medium	Medium	High	Medium
85	Extreme	High	Medium	Low	High
86	Extreme	High	Medium	High	High
87	Extreme	Extreme	Medium	Low	Extreme
88	Extreme	Extreme	Medium	High	Extreme
89	Extreme	Low	High	Low	High
90	Extreme	Low	High	High	High
91	Extreme	Medium	High	Low	High
92	Extreme	Medium	High	High	High
93	Extreme	High	High	Low	High
94	Extreme	High	High	High	High
95	Extreme	Extreme	High	Low	Extreme
96	Extreme	Extreme	High	High	Extreme

Fuzzy Inference System Elevation Uncertainty Model

A fuzzy inference system uses combinations of known parameters, such as slope and point density, that affect survey or interpolation accuracy to generate a single elevation uncertainty estimate on a pixel-by-pixel basis using empirically derived values and knowledge-based relationships between inputs and uncertainty. We used the Geomorphic Change Detection software (http://gcd.riverscapes.xyz/) and followed the procedures outlined by Wheaton and others (2010), Bangen and others (2016), and Kaplinski and others (2017) to develop and apply the FIS error models. Input and output variable ranges are binned into membership functions that are subdivided into classes. For any combination of input variables, applicable membership functions are selected and combined using a rule table to yield a fuzzy estimate of elevation uncertainty. The rule table codifies all combinations of input membership function relationships and determines the location on the output elevation uncertainty membership function. For example, if a survey area has a relatively low slope and a high point density, it should have a relatively low elevation uncertainty. In contrast, an area with greater slope and a lower point density should have a relatively higher elevation uncertainty. The fuzzy elevation uncertainty is then translated into a numeric uncertainty estimate by computing the centroid of the applicable elevation uncertainty membership functions. The elevation uncertainty output is calculated for each grid cell and tabulated in a raster surface, concurrent with the DEM. A detailed discussion of FIS error modeling is available in Wheaton and others (2010), Jang and Gully (2014), Bangen and others (2016), and the Geomorphic Change Detection website (http://gcd.riverscapes.xyz/).

A FIS model was developed for each type of data collection (digital surface model, multibeam, singlebeam, total station) within the Glen Canyon reach, and the model outputs were combined in one raster surface. The FIS model for digital surface model survey areas used two input membership functions (slope and point density; fig. 6). The FIS model for multibeam sonar survey areas used four input membership functions (slope, interpolation error, point density, and roughness; fig. 7), and the FIS models for singlebeam and total station survey areas used three input membership functions (slope, interpolation error, and point density; figs. 8, 9). All FIS models developed in this study use a Mamdani FIS type, minimum rule implication method, maximum aggregation method, centroid defuzzification method, and trapezoidal membership function shape (Jang and Gully, 2014).

Fuzzy Inference System Input

Input membership functions were derived from either the DEM or raw survey point data. Membership function classes are defined using the statistical distribution of the input variable observed across the study area. Each input was represented as a 1-m raster.

The contribution of topographic complexity to elevation uncertainty was modeled as an input membership function by using the DEM slope and surface roughness. DEM slope was used for all four input membership functions and roughness was only used for the multibeam survey FIS. DEM surface slope (in degrees) was derived for each 1-m grid cell by calculating the maximum rate of elevation change within a 3 by 3 cell neighborhood (Wheaton and others, 2010). Surface roughness was calculated using the methods of Buscombe (2016) for each 1-m grid cell using the 0.25-m grid of multibeam elevations.

Differences in point density arise as a result of the different sampling strategies of each data-collection method. Point density was calculated from the survey point cloud using a 5-m radius circular neighborhood. The four data-collection methods have unique distributions, and separate input membership functions were developed for each data-collection type.

Interpolation uncertainty represents the error introduced during interpolation of the irregularly spaced points that are explicitly represented in the TIN model to produce a regularly spaced grid of elevations (for example, a raster DEM). Interpolation uncertainty was derived by calculating the elevation difference between the final DEM and input point data.

Fuzzy Inference System Output

The FIS output elevation uncertainty membership functions are used in combination with the rules table to generate a single elevation uncertainty estimate for each grid cell. Defining the output elevation uncertainty categories is an iterative process that incorporates expert knowledge of the survey methods and the terrain surveyed, and that is calibrated to an independent estimate of elevation uncertainty. The minimum elevation uncertainty (or lower end of the output categories) was defined by the measurement uncertainty for each data-collection type (table 1, fig 4). The maximum elevation uncertainty was set to the maximum local relief observed in the study reach for each data-collection type. For the digital surface model survey area, we set the maximum relief to 5 m, which is an estimate of the maximum relief of the digital surface model area within the alluvial portion of the river valley. Because the digital surface model survey area also encompasses the cliffs surrounding the river valley, this biases the uncertainty output to the alluvial portion and underestimates the uncertainty output for the cliff and bedrock areas. However, since the focus of research and management activities is confined to the alluvial valley, we chose to limit the uncertainty maximum relief to within valley alluvial surfaces. Other category boundaries (“low”, “medium”, “high”, and “extreme”) were defined by empirical relationships pertinent to each data-collection type.

Once the minimum (measurement uncertainty) and maximum (bank height) levels were established, the output membership functions for each data-collection type were calibrated to an independent source of uncertainty. For

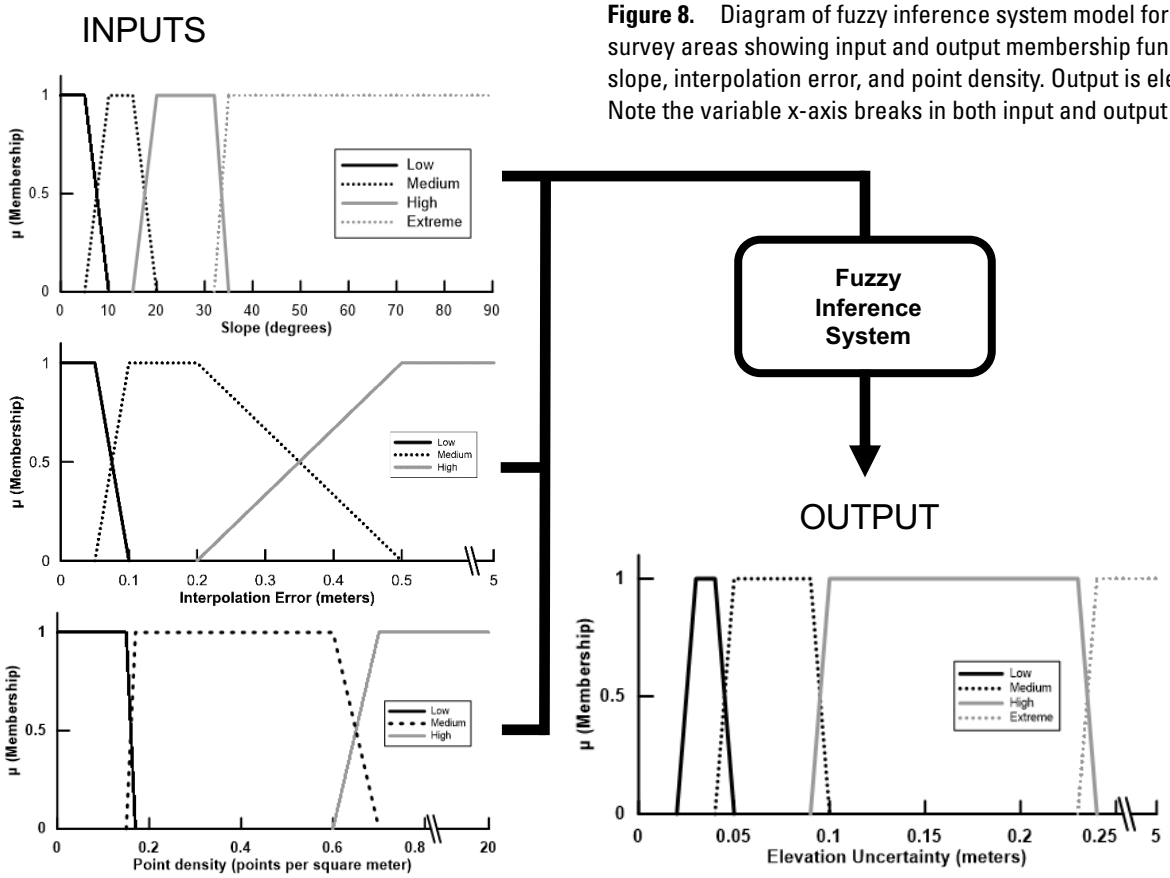

Figure 8. Diagram of fuzzy inference system model for singlebeam sonar survey areas showing input and output membership functions. Inputs are slope, interpolation error, and point density. Output is elevation uncertainty. Note the variable x-axis breaks in both input and output functions.

Table 4. Three-input fuzzy inference system ruleset for singlebeam sonar surveys.

Rule	Inputs			Output (meters)
	Slope (degrees)	Interpolation (meters)	Point Density (points per square meter)	
1	Low	Low	Low	Medium
2	Low	Medium	Low	Medium
3	Low	High	Low	High
4	Low	Low	Medium	Low
5	Low	Medium	Medium	Medium
6	Low	High	Medium	Medium
7	Low	Low	High	Low
8	Low	Medium	High	Medium
9	Low	High	High	Medium
10	Medium	Low	Low	Medium
11	Medium	Medium	Low	Medium
12	Medium	High	Low	High
13	Medium	Low	Medium	Low
14	Medium	Medium	Medium	Medium
15	Medium	High	Medium	High
16	Medium	Low	High	Low
17	Medium	Medium	High	Medium

Table 4. Three-input fuzzy inference system ruleset for singlebeam sonar surveys.—Continued

Rule	Inputs			Output (meters)
	Slope (degrees)	Interpolation (meters)	Point Density (points per square meter)	
18	Medium	High	High	High
19	High	Low	Low	Medium
20	High	Medium	Low	High
21	High	High	Low	High
22	High	Low	Medium	Medium
23	High	Medium	Medium	High
24	High	High	Medium	High
25	High	Low	High	Medium
26	High	Medium	High	High
27	High	High	High	High
28	Extreme	Low	Low	High
29	Extreme	Medium	Low	High
30	Extreme	High	Low	Extreme
31	Extreme	Low	Medium	Medium
32	Extreme	Medium	Medium	High
33	Extreme	High	Medium	Extreme
34	Extreme	Low	High	Medium
35	Extreme	Medium	High	High
36	Extreme	High	High	Extreme

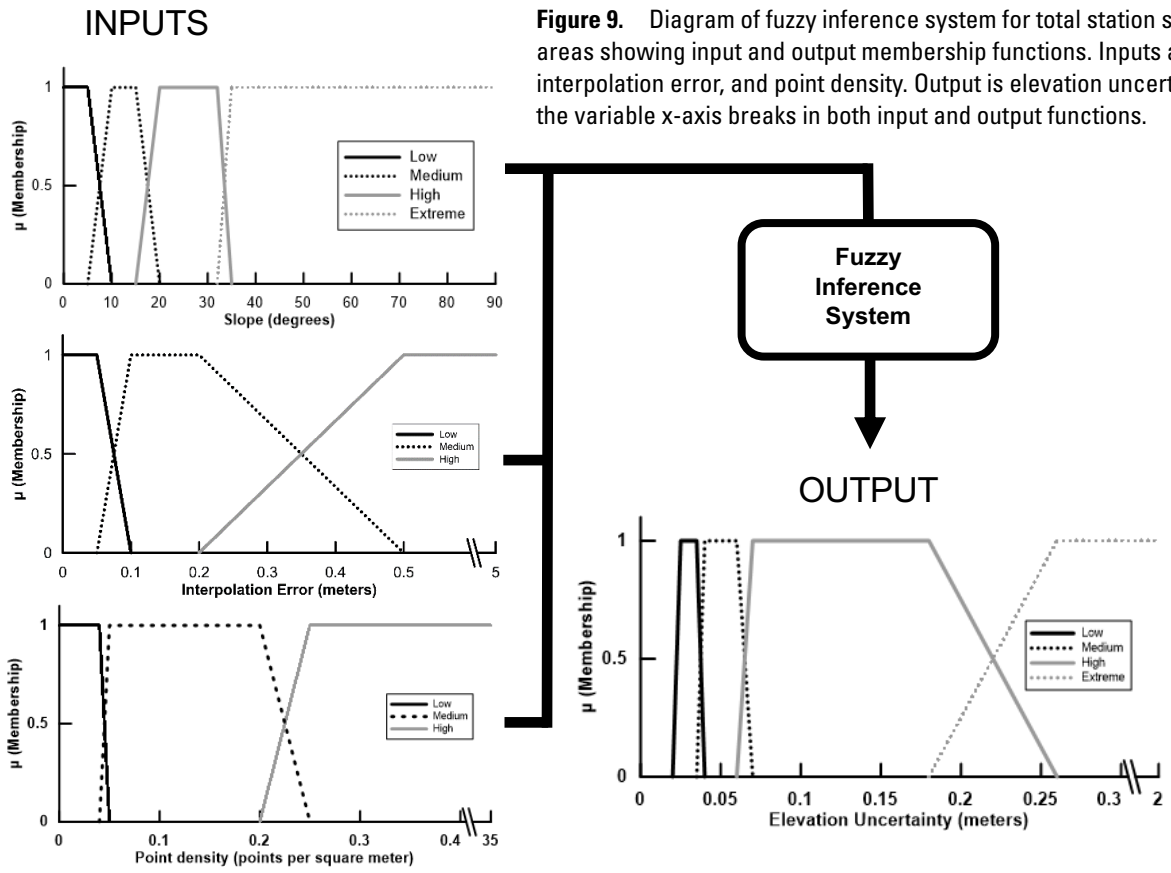

Figure 9. Diagram of fuzzy inference system for total station survey areas showing input and output membership functions. Inputs are slope, interpolation error, and point density. Output is elevation uncertainty. Note the variable x-axis breaks in both input and output functions.

Table 5. Three-input fuzzy inference system ruleset for total station surveys.

Rule	Inputs			Output (meters)
	Slope (degrees)	Interpolation (meters)	Point density (points per square meter)	
1	Low	Low	Low	Low
2	Low	Medium	Low	Medium
3	Low	High	Low	High
4	Low	Low	Medium	Low
5	Low	Medium	Medium	Medium
6	Low	High	Medium	Medium
7	Low	Low	High	Low
8	Low	Medium	High	Medium
9	Low	High	High	Medium
10	Medium	Low	Low	Medium
11	Medium	Medium	Low	High
12	Medium	High	Low	High
13	Medium	Low	Medium	Low
14	Medium	Medium	Medium	Medium
15	Medium	High	Medium	High
16	Medium	Low	High	Low
17	Medium	Medium	High	Medium
18	Medium	High	High	High
19	High	Low	Low	High
20	High	Medium	Low	High
21	High	High	Low	High
22	High	Low	Medium	Medium
23	High	Medium	Medium	High
24	High	High	Medium	High
25	High	Low	High	Medium
26	High	Medium	High	High
27	High	High	High	High
28	Extreme	Low	Low	High
29	Extreme	Medium	Low	High
30	Extreme	High	Low	Extreme
31	Extreme	Low	Medium	High
32	Extreme	Medium	Medium	High
33	Extreme	High	Medium	Extreme
34	Extreme	Low	High	Medium
35	Extreme	Medium	High	High
36	Extreme	High	High	Extreme

multibeam and singlebeam sonar survey areas, the output membership functions derived by Kaplinski and others (2017) were applied. These membership functions were derived for a topographically complex site with a variety of channel bed features that is characteristic of the entire study reach. An independent source of uncertainty does not exist for the digital surface model survey area. So, the membership functions used for multibeam and SB survey areas were scaled to the digital surface model survey area by adjusting the category boundaries by the difference between the measurement uncertainty standard deviations (about 0.07 m). Total station data were calibrated using the values derived by Wheaton and others (2010). Rule tables were developed for each FIS (tables 2–5) and used in combination with the FIS input and output membership functions to generate a spatially distributed elevation uncertainty surface of the entire study reach.

Results

A 1-m-resolution DEM was constructed for a 15.84-mi study reach along the Colorado River between Glen Canyon Dam and Lees Ferry, Arizona, using data collected between May 2013 and February 2016. In addition to the aerial overflight data, data from 35 multibeam surveys, 14 singlebeam surveys, and 26 total station surveys were collected.

The DEM covers an area of 13.704 km^2 that contains 100 percent of the channel (by area) within the study reach. Digital surface model data covered 75 percent of the DEM area, multibeam surveys (and bed-substrate classifications derived from the multibeam data) covered 23 percent of the DEM, and singlebeam and total station surveys each covered 1 percent of the DEM area. The DEM is available in digital format in the companion data release (Kaplinski and others, 2022; available at https://doi.org/10.5066/P98GFP93).

A 1-m resolution grid of spatially distributed uncertainty was created to accompany the DEM by using fuzzy interference system (FIS) modeling. FIS models, developed for each type of data collection (digital surface model, multibeam, singlebeam, and total station surveys) and based on surfaces derived from the DEM and survey data (slope, roughness, points density, interpolation uncertainty), were used to generate a spatially variable elevation uncertainty surface. Within the digital surface model survey area, the two-input FIS model produced elevation uncertainties that ranged from 0.06 to 2.666 m, with a median of 0.097 m (fig. 10*A*). For the multibeam survey area, the four-input FIS model produced per-cell elevation uncertainties that ranged from 0.035 to 2.617 m, with a median of 0.057 m (fig. 10*B*). The singlebeam and total station survey areas have median uncertainties of 0.075 m and 0.030 m, respectively (fig. 10*C* and 10*D*). The FIS uncertainty estimates are available in

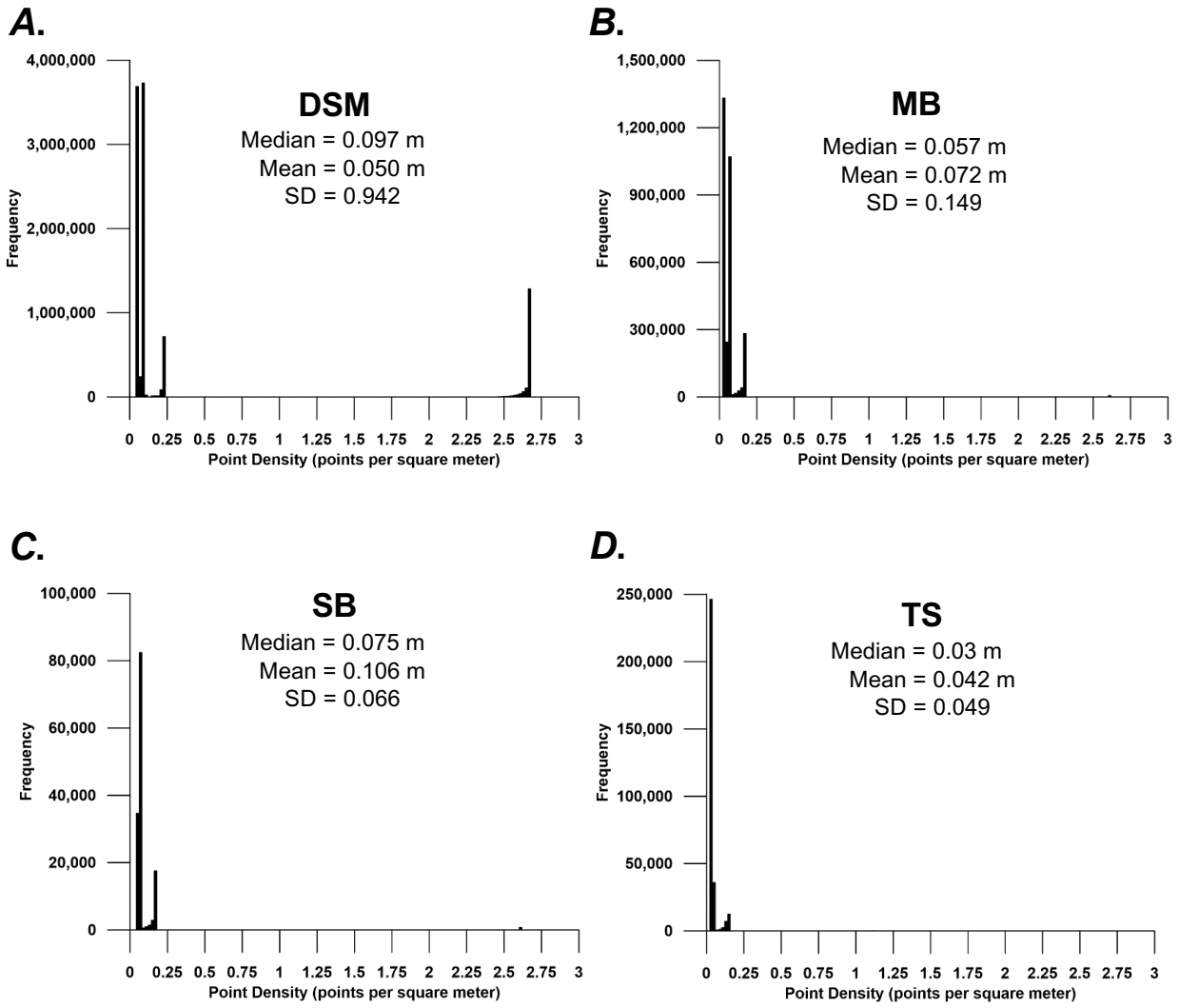

Figure 10. Fuzzy inference system (FIS) output (elevation uncertainty) distributions and summary statistics for each survey type. *A*, FIS output distributions and summary statistics for digital surface model (DSM) survey area. *B*, FIS output distributions and summary statistics for multibeam (MB) survey area. *C*, FIS output distributions and summary statistics for singlebeam (SB) survey area. *D*, FIS output distributions and summary statistics for total station (TS) survey area. Median, mean, and standard deviation (SD) in meters.

digital format in the companion data release (Kaplinski and others, 2022; https://doi.org/10.5066/P98GFP93).

Bed-substrate classification maps were produced at 1-m resolution using the methods of Buscombe and others (2017). The maps show that 23 percent of the channel is densely vegetated (V), 37 percent is sparsely vegetated (vSG), 24 percent is unvegetated gravel and (or) cobble (Gc), and 16 percent is unvegetated cobble, boulder, and (or) bedrock (cBR). The bed-substrate classification maps are available in digital format in the companion data release (Kaplinski and others, 2022; https://doi.org/10.5066/P98GFP93).

Conclusions

The results from this study will inform ongoing efforts to assess the effects of Glen Canyon Dam operations on the status and trends of sediment resources in the Colorado River ecosystem. The DEM and bed-substrate classifications will be used by researchers to map the spatial characteristics of geomorphic change. The data will also provide valuable information for the development of hydraulic and morphodynamic models, characterize the spatial distribution of benthic habitat for aquatic and riparian ecosystem investigations, and provide the recreation community with a complete topographic map of the Colorado River corridor in Glen Canyon.

Acknowledgments

This study was made possible by the hard work of the numerous members of the field survey team. In particular, we thank Dave Foster, Seth Felder, Rob Ross, Rod Parnell, Karen Koestner, and Ryan Seumptewa for their great attitude and expertise in the field. James Hensleigh offered extensive database and GIS services and Rebecca Beers contributed many hours of processing in the laboratory. Reviews by Paul Kinzel and Carrie Elliott are gratefully acknowledged.

References Cited

Bangen, S., Hensleigh, J., McHugh, P., and Wheaton, J., 2016, Error modeling of DEMs from topographic surveys of rivers using fuzzy inference systems: Water Resources Research, v. 52, no. 2, p. 1176–1193, https://doi.org/10.1002/2015WR018299.

Brasington, J., Langham, J., and Rumsby, B., 2003, Methodological sensitivity of morphometric estimates of coarse fluvial sediment transport: Geomorphology, v. 53, nos. 3–4, p. 299–316, https://doi.org/10.1016/S0169-555X(02)00320-3.

Buscombe, D., 2016, Spatially explicit spectral analysis of point clouds and geospatial data: Computers and Geosciences, v. 86, p. 92–108, https://doi.org/10.1016/j.cageo.2015.10.004.

Buscombe, D., Grams, P.E., and Kaplinski, M.A., 2014a, Characterizing riverbed sediment using high-frequency acoustics—1. Spectral properties of scattering: Journal of Geophysical Research—Earth Surface, v. 119, no. 12, p. 2674–2691, https://doi.org/10.1002/2014JF003189.

Buscombe, D., Grams, P.E., and Kaplinski, M.A., 2014b, Characterizing riverbed sediment using high-frequency acoustics—2. Scattering signatures of Colorado River bed sediment in Marble and Grand Canyons: Journal of Geophysical Research—Earth Surface, v.119, no. 12, p. 2692–2710, https://doi.org/10.1002/2014JF003191.

Buscombe, D., Grams, P.E., and Kaplinski, M.A., 2017, Compositional signatures in acoustic backscatter over vegetated and unvegetated mixed sand-gravel riverbeds: Journal of Geophysical Research—Earth Surface, v.122, no. 10, p. 1771–1793, https://doi.org/10.1002/2017JF004302.

Doyle, D.R., 1994, Development of the National Spatial Reference System: National Geodetic Survey Publications web page, accessed August 26, 2021, at https://www.ngs.noaa.gov/PUBS_LIB/develop_NSRS.html.

Durning, L.E., Sankey, J.B., Bedford, A., and Sankey, T.T., 2018, Riparian species vegetation classification data for the Colorado River within Grand Canyon derived from 2013 airborne imagery: U.S. Geological Survey data release, accessed August 26, 2021, at https://doi.org/10.5066/P9OUB1RS.

Durning, L.E., Sankey, J.B., Davis, P.A., and Sankey, T.T., 2016a, Four-band image mosaic of the Colorado River corridor downstream of Glen Canyon Dam in Arizona, derived from the May 2013 airborne image acquisition: U.S. Geological Survey Data Series 1027, https://doi.org/10.3133/ds1027.

Durning, L.E., Sankey, J.B., Davis, P.A., and Sankey, T.T., 2016b, Four band image mosaic of the Colorado River corridor in Arizona—2013 [including Accuracy Assessment Data]: U.S. Geological Survey data release, accessed August 26, 2021, at https://doi.org/10.5066/F7TX3CHS.

Graf, J.B., Jansen, S.M.D., Fisk, G.G., and Marlow, J.E., 1995, Topography and bathymetry of the Colorado River, Grand Canyon National Park, Little Colorado River confluence to Tanner Rapids: U.S. Geological Survey Open-File Report 95-726, https://doi.org/10.3133/ofr95726.

Grams, P.E., Schmidt, J.C., and Topping, D.J., 2007, The rate and pattern of bed incision and bank adjustment on the Colorado River in Glen Canyon downstream from Glen Canyon Dam, 1956–2000: Geological Society of America Bulletin, v. 119, nos. 5–6, p. 556–575, https://doi.org/10.1130/B25969.1.

Gushue, T.M., 2019, Colorado River Mile System, Grand Canyon, Arizona: U.S. Geological Survey data release, accessed August 26, 2021, at https://doi.org/10.5066/P9IRL3GV.

Heritage, G., and Large, A.R.G., eds., 2009, Laser scanning for the environmental sciences: Chichester, United Kingdom, Wiley, 288 p.

Jang, J., and Gulley, N., 2014, Fuzzy logic toolbox—User guide: Natick, Mass., Mathworks, 328 p.

Kaplinski, M., Hazel, J.E., Jr., Grams, P.E., and Davis, P., 2014, Monitoring fine-sediment volume in the Colorado River ecosystem, Arizona—Construction and analysis of digital elevation models: U.S. Geological Survey Open-File Report 2014–1052, 29 p., https://doi.org/10.3133/ofr20141052.

Kaplinski, M., Hazel, J.E., Jr., Grams, P.E., Gushue, T., Buscombe, D.D., and Kohl, K., 2022, Channel mapping Glen Canyon Dam to Lees Ferry in Glen Canyon National Recreation Area—Data: U.S. Geological Survey data release, https://doi.org/10.5066/P98GFP93.

Kaplinski, M., Hazel, J.E., Jr., Grams, P.E., Kohl, K., Buscombe, D.D., and Tusso, R.B., 2017, Channel mapping river miles 29–62 of the Colorado River in Grand Canyon National Park, Arizona, May 2009: U.S. Geological Survey Open-File Report 2017-1030, 35 p., https://doi.org/10.3133/ofr20171030.

Kaplinski, M., Hazel, J.E., Jr., Parnell, R., Breedlove, M., Kohl, K., and Gonzales, M., 2009, Monitoring fine-sediment volume in the Colorado River ecosystem, Arizona—Bathymetric survey techniques: U.S. Geological Survey Open-File Report 2009–1207, 33 p., https://doi.org/10.3133/ofr20091207.

Kennedy, T.A., Muehlbauer, J.D., Yackulic, C.B., Lytle, D.A., Miller, S.W., Dibble, K.L., Kortenhoeven, E.W., Metcalfe, A.N., and Baxter, C.V., 2016, Flow management for hydropower extirpates aquatic insects, undermining river food webs: BioScience, v. 66, no. 7, p. 561–575, https://doi.org/10.1093/biosci/biw059.

Korman, J., Yard, M.D., and Kennedy, T.A., 2017, Trends in rainbow trout recruitment, abundance, survival, and growth during a boom-and-bust cycle in a tailwater fishery: Transactions of the American Fisheries Society, v. 146, no. 5, p. 1043–1057, https://doi.org/10.1080/00028487.2017.1317663.

Lane, S.N., 1998, The use of digital terrain modelling in the understanding of dynamic river channel systems, in Lane, S.N., Richards, K., and Chandler, J., eds., Landform monitoring, modelling, and analysis: Chichester, United Kingdom, Wiley, p. 311–342.

Lane, S.N., Westaway, R.M., and Hicks, D.M., 2003, Estimation of erosion and deposition volumes in a large, gravel-bed, braided river using synoptic remote sensing: Earth Surface Processes and Landforms, v. 28, no. 3, p. 249–271, https://doi.org/10.1002/esp.483.

Liu, X., Shi, C., Zhou, Y., Gu, Z., and Li, H., 2019, Response of erosion and deposition of channel bed, banks and floodplains to water and sediment changes in the Lower Yellow River, China: Water, v. 11, no. 2, 15 p., https://doi.org/10.3390/w11020357.

Pemberton, E.L., 1976, Channel change in the Colorado River below Glen Canyon Dam, in Symposium 5—Channel adjustments of Proceedings of the Third Federal Interagency Sedimentation Conference, Denver, Colo., March 22–25, 1976: Washington, D.C., U.S. Subcommittee on Sedimentation, p. 61–73.

Peuker, T.K., Fowler, R.J., Little, J.J., and Mark, D.M., 1978, The triangulated irregular network, in Proceedings of the Digital Terrain Models (DTM) Symposium, St. Louis, Mo., May 9–11, 1978: Falls Church, Va., American Society of Photogrammetry, p. 516–540.

Ralston, B.E., Cobb, N.S., Brantley, S.L., Higgins, J., and Yackulic, C.B., 2017, Taxonomic and compositional differences of ground-dwelling arthropods in riparian habitats in Glen Canyon, Arizona, USA: Western North American Naturalist, v. 77, no. 3, p. 369–384, https://doi.org/10.3398/064.077.0309.

Sankey, J.B., Ralston, B.E., Grams, P.E., Schmidt, J.C., and Cagney, L.E., 2015, Riparian vegetation, Colorado River, and climate—Five decades of spatiotemporal dynamics in the Grand Canyon with river regulation: Journal of Geophysical Research—Biogeosciences, v. 120, no. 8, p. 1532–1547, https://doi.org/10.1002/2015JG002991.

Stem, J.E., 1989, State Plane Coordinate System of 1983 (revised 1990): National Oceanic and Atmospheric Administration Manual NOS NGS 5, 119 p., accessed August 26, 2021, at https://www.ngs.noaa.gov/PUBS_LIB/ManualNOSNGS5.pdf. [Reprinted 1995.]

Topping, D.J., Schmidt, J.C., and Vierra, L.E., Jr., 2003, Computation and analysis of the instantaneous-discharge record for the Colorado River at Lees Ferry, Arizona—May 8, 1921, through September 30, 2000: U.S. Geological Survey Professional Paper 1677, 118 p., https://doi.org/10.3133/pp1677.

U.S. Army Corps of Engineers, 2013, Hydrographic surveying: U.S Army Corps of Engineers Engineer Manual 1110-2-1003, 506 p., accessed August 26, 2021, at http://www.publications.usace.army.mil/Portals/76/Publications/EngineerManuals/EM_1110-2-1003.pdf.

U.S. Department of the Interior, 1995, Operation of Glen Canyon Dam final environmental impact statement, Colorado River Storage Project, Coconino County, Arizona: Salt Lake City, Utah, U.S. Bureau of Reclamation, Upper Colorado Regional Office, 337 p.

U.S. Geological Survey, 2017, 1/3rd arc-second Digital Elevation Models (DEMs)—USGS National Map 3DEP downloadable digital collection: U.S. Geological Survey dataset, accessed March 23, 2022, at https://www.usgs.gov/3d-elevation-program.

Webb, R.H., Schmidt, J.C., Marzolf, G.R., and Valdez, R.A., eds., 1999, The controlled flood in Grand Canyon: American Geophysical Union Geophysical Monograph 110, 367 p., https://doi.org/10.1029/GM110.

Wheaton, J.M., Brasington, J., Darby, S.E., and Sear, D.A., 2010, Accounting for uncertainty in DEMs from repeat topographic surveys—Improved sediment budgets: Earth Surface Processes and Landforms, v. 35, no. 2, p. 136–156, https://doi.org/10.1002/esp.1886.

Williams, G.P., 1978, Hydraulic geometry of river cross sections—Theory of minimum variance: U.S. Geological Survey Professional Paper 1029, 47 p., https://doi.org/10.3133/pp1029.

Willmott, C.J., and Matsuura, K., 2005, Advantages of the mean absolute error (MAE) over the root mean square error (RMSE) in assessing average model performance: Climate Research, v. 30, p. 79–82, https://doi.org/10.3354/CR030079.

Zilkoski, D.B., D'Onofrio, J.D., and Frakes, S.J., 1997, Guidelines for establishing GPS-derived ellipsoid heights [standards—2 cm and 5 cm] (ver. 4.3): National Oceanic and Atmospheric Administration Technical Memorandum NOS NGS 58, 22 p., https://doi.org/10.25607/OBP-152.

Moffett Field Publishing Service Center, California
Manuscript approved for publication May 25, 2022
Edited by Timothy Herold
Layout and design by Kimber Petersen

ISSN 2331-1258 (online)
https://doi.org/10.3133/ofr20221057